Article:
Lu, X., Xie, P. orcid.org/0000-0001-7156-7061, Ingham, D.B. et al. (2 more authors) (2018) A porous media model for CFD simulations of gas-liquid two-phase flow in rotating packed beds. Chemical Engineering Science, 189. pp. 123-134. ISSN 0009-2509

https://doi.org/10.1016/j.ces.2018.04.074

Chemical Engineering Science 189 (2018) 123–134

Contents lists available at ScienceDirect

Chemical Engineering Science

journal homepage: www.elsevier.com/locate/ces

A porous media model for CFD simulations of gas-liquid two-phase flow in rotating packed beds

X. Lu, P. Xie, D.B. Ingham, L. Ma *, M. Pourkashanian

Energy 2050, Mechanical Engineering, Faculty of Engineering, University of Sheffield, Sheffield S10 2TN, UK

HIGHLIGHTS

- A new porous media model is proposed for an Eulerian simulation of RPBs.
- The predicted liquid holdup distribution agrees very well with experimental data.
- The new porous media model is the most accurate among current investigated models.

ARTICLE INFO

Article history:
Received 23 February 2018
Received in revised form 23 April 2018
Accepted 30 April 2018
Available online 23 May 2018

Keywords:
Rotating packed bed
CFD simulation
Porous media model
Gas-liquid two-phase flow

ABSTRACT

The rotating packed bed (RPB) is a promising advanced reactor used in industrial gas-liquid two-phase reaction processes because of its high phase contact efficiency and mixing efficiency. Investigation of RPBs using CFD simulations will improve the understanding of physical behaviours of gas and liquid flows in such reactors. Currently, CFD simulations on the RPBs only focus on the volume of fluid (VOF) method. However, the VOF method is not suitable for simulations of pilot-scale 2D and 3D RPBs due to the limitations in computer resources, while the Eulerian method using a porous media model is a promising alternative method but it is rarely reported. The reason is that there are no suitable porous media models that accurately describe the drag force between the gas and liquid, the gas and solids and the liquid and solids due to the high porosity and the stacked wire screen packing used in RPBs. Therefore, the purpose of this paper is to propose a new model for modelling RPBs. The new proposed model is based on the Kołodziej high porosity wire screen one-phase porous media model. In this work, two experimental counter-current gas–liquid flow cases from the literatures have been used for validating the CFD simulation results. Finally, the new model has been compared with the current porous media models for traditional spherical or structured slit packed beds, which are the Attou, Lappalainen, Iliuta and Zhang models. The simulation results show that the proposed new model is the most appropriate and accurate model for the simulation of RPBs among all the models investigated in this paper.

1. Introduction

The rotating packed bed (RPB) was first proposed and developed by Prof. Colin Ramshaw in the 1980s (Ramshaw and Mallinson, 1981; Ramshaw, 1983) and a typical RPB is shown in Fig. 1. This system comprises of a rotating packed bed, static chamber, gas inlet tube situated on the top of the static chamber, a gas outlet tube connected to the central inner part of the rotating packed bed, a liquid jet splashing or spraying liquid from the central inner part of the rotating packed bed, and a liquid outlet tube located at the bottom of the static chamber. In this reactor, screens, meshes or gauzes are often used as the packing materials and this is because these packing materials have low flow resistance, high specific area and high capability to thinning the liquid film and breaking down the liquid droplets. During the operation, the gas and liquid can flow through the rotating packed bed co-currently, counter-currently or cross-currently in this reactor. The liquid can be observed to flow in the form of a rivulet flow, film flow and droplet flow. The RPB can create a high centrifugal acceleration, and this produces much thinner films (1–10 μm) and smaller droplets (10–100 μm) with a high interfacial area between the gas and liquid phases (Yan et al., 2014; Zhao et al., 2016). It was found that the mass transfer coefficient was enhanced by a factor of 27–44 higher than that in the conventional packed columns and this is because the mass transfer between the gas and liquid occurs on the thin film located on the surface of the packed materials or in smaller droplets (Chen et al., 2006). In addition to the higher mass

* Corresponding author.
E-mail address: lin.ma@sheffield.ac.uk (L. Ma).

https://doi.org/10.1016/j.ces.2018.04.074
0009-2509/

Nomenclature

A	constant in the viscous term of the Ergun type equation
A_d	total projected area of the droplets in a given control volume, m^2
a_S	specific area of the dry packing materials, m^2/m^3
a'_S	specific area of the wet wires, m^2/m^3
B	constant in the inertial term of the Ergun type equation
C_2	inertial resistance coefficient in the porous media equation
C_f	interphase friction coefficient
D_d	droplet diameter, m
D_h	hydraulic diameter, m
D_o	outer diameter of the tube, m
d_p	equivalent sphere diameter of the packing materials, m
d_w	wire diameter, m
d'_w	wire and liquid film diameter, m
E_1	one phase specific Ergun coefficient
E_2	one phase specific Ergun coefficient
$E_{\mu,i}$	phase specific Ergun coefficient
$E_{\rho,i}$	phase specific Ergun coefficient
F_{drag}	drag force, $N\ m^{-3}$
F'_{GL}	interphase momentum exchange coefficient, $kg\ m^{-3}\ s^{-1}$
F_{GL}	drag force between the gas and liquid, $N\ m^{-3}$
F_{GS}	interaction force between the gas and solids of the packing materials, $N\ m^{-3}$
F_{LS}	interaction force between the liquid and solids of the packing materials, $N\ m^{-3}$
F_{int}	total interaction force for the gas phase or liquid phase, $N\ m^{-3}$
f	friction factor
f_{app}	Fanning friction factor for developing laminar flow
f_d	friction factor of the droplets
f_e	wetting efficiency
f_t	Fanning friction factor for the developing turbulence flow
f_τ	friction factor
GFR	volumetric flow rate of the gas, m^3/s
g	acceleration due to gravity, $m\ s^{-2}$
g_c	centrifugal acceleration, $m\ s^{-2}$
g_0	characteristic centrifugal acceleration (=100 $m\ s^{-2}$), $m\ s^{-2}$
H	height of packed bed, m
h	thickness of rotating packed bed, m
h_L	liquid holdup
n	rotation speed, rpm
P	pressure, Pa
P_t	tube pitch
Q_i	volume flow rate, m^3/s
R_l	volume fraction of liquid phase
r	radial coordinate, m
r_i	inner radius of the packed bed, m
r_o	outer radius of the packed bed, m
Δr	radial separation, m
S_i	momentum source, $N\ m^{-3}$
$S_{m,i}$	mass source, $kg\ m^{-3}\ s^{-1}$
T_i	i phase specific tortuosity
T_0	empty bed tortuosity
U	liquid flow rate per unit area, $m\ s^{-1}$
U_0	characteristic flow rate per unit area (=1 $cm\ s^{-1}$), $m\ s^{-1}$
V	volume, m^3
v	velocity, $m\ s^{-1}$
v_e	effective velocity, $m\ s^{-1}$
v_p	velocity magnitude, $m\ s^{-1}$
x	axial coordinate, m
Δx	axial separation, m
z	tangential coordinate, m

Greek

α_i	phase fraction
α_{gs}	gas saturation
α_1	viscous resistance coefficient in porous media equation
β	local porosity
β_1	gas-packing slip parameter
β_2	gas-liquid slip parameter
βt	porosity in tube bundle region
χ^+	dimensionless channel length
ε_i	volume fraction of the i phase
μ_i	dynamic viscosity of the i phase, Pa s
ν	kinematic viscosity, $m^2\ s^{-1}$
ν_0	characteristic kinematic viscosity (= $1.0 \times 10^{-6}\ m^2\ s^{-1}$), $m^2\ s^{-1}$
θ	angle between the flow direction and the bed axis, °
ρ_i	density of the i phase, $kg\ m^{-3}$
σ	surface tension, $N\ m^{-1}$
σ_c	critical surface tension, $N\ m^{-1}$
τ	bed tortuosity factor
τ_m	micromixing time, s
ω	rotation speed, $rad\ s^{-1}$
ξ	pressure loss coefficient

Dimensionless groups

Fr	Froude number
Re	Reynold number
We	Webber number

Subscripts

G	gas phase
i	= G, L
K	Kołodziej model
L	liquid phase
r	radial coordinate
S	solids phase for packing materials
x	axial coordinate
z	tangential coordinate

transfer coefficient, there is a higher efficient micromixing, which is intensified by the stirring caused by the rotation and this is another advantage of the RPB. Yang et al. (2005) estimated the micromixing time τ_m in the RPB to be at the level of 10^{-4} s and demonstrated that the RPB has a large advantage in improving the micromixing efficiency over other reactors. Nowadays, many researchers have carried out investigations on RPBs in the following fields: (i) flow hydrodynamics, especially the pressure drop across the bed (Guo et al., 1997; Chandra et al., 2005); (ii) mass transfer (Jiao et al., 2010; Chen et al., 2011); (iii) liquid holdup (Lin et al., 2000; Băsić and Duduković, 1995); (iv) effective interfacial area (Luo et al., 2012); and (v) micromixing (Yang et al., 2005; Chen et al., 2004). Currently, the RPBs have already been widely applied in many chemical processes, e.g. distillation (Lin et al., 2002), synthesis of nano-fibers of aluminum hydroxide (Chen et al., 2003), combined photolysis and catalytic ozonation of dimethyl phthalate (Chang et al., 2009), biodiesel production (Chen et al., 2010), removal of volatile organic compounds (VOCs) from waste gas streams (Lin et al., 2006), removal of hexavalent chromium by a biosorption process (Panda et al., 2011), preparation of nano-particles such as ZnO/SnO_2 as photocatalysts (Lin and Chiang, 2012) or nano-$CaCO_3$ (Sun et al., 2011) and H_2S or

CO_2 adsorption (Jassim et al., 2007; Qian et al., 2010). The RPB is also a promising reactor for CO_2 capture in the post combustion of a power plant because it demonstrates that the RPB could reduce the reactor size and energy, operation space and have a highly efficient operation in comparison with the traditional packed beds or trickle beds (Jassim et al., 2007).

CFD investigations of RPBs assist in the understanding of the physical behaviour of gas-liquid interactions and mechanisms, and assist in the scale up of the reactor from lab-scale to industrial scale. The most popular CFD simulation methods for gas-liquid two-phase flows are the Euler-Euler and VOF methods and these are based on the macroscale or mesoscale. The other important simulation methods are the direct numerical simulation (DNS) methods that are based on the microscale or mesoscale, such as the front tracking (FT) method (Dijkhuizen et al., 2010). These methods can simulate a very small bubble with high surface tension and accurately capture the phase interface without any volume loss and the creation of spurious currents. The lattice Boltzmann method (LBM) can bridge the macroscale and microscale flows and accurately simulate the interfaces in bubble and multiphase flows in porous media (Sankaranarayanan et al., 1999; Li et al., 2013; Shu and Yang, 2013).

At present, CFD simulations of the liquid flow in RPBs only focus on the VOF method and the packing wire mesh that was assumed to be square or circular blocks in 2D models (Yang et al., 2010; Shi et al., 2013; Xie et al., 2017). The formation of the film and droplets can clearly be observed during the transient simulations. For example, Yang et al. (2016) used this method to investigate the liquid holdup and mass transfer of the dissolved oxygen released into the gas phase under different rotation speeds and liquid flow rates. The advantages of the VOF method and the method of blocks as the packing wires are as follows: (i) three typical flows (film, rivulet, and droplet) can be described and observed directly, (ii) maldistribution of liquid can be obtained, (iii) the simulation does not require to estimate the interaction force between the phases; and (iv) it is a simple model with the gas and liquid treated as one mixture phase and easily performed compared to the Euler-Euler model. The main disadvantages of this method are (i) it requires a very small grid size to capture the droplets and film, and therefore it cannot simulate 3D or large pilot scale RPBs because of computer resource and time limitations. For example, a 3D model for a small RPB rig (inner radius: 30 mm, outer radius: 160 mm and axial height: 50 mm) requires 1,071,338 tetrahedral and 26,190 pyramid grids (Yang et al., 2010), and (ii) transient simulations have to be performed with the VOF method, which generally takes a much longer time than steady-state simulations, even though, for most of the cases investigated, the flow in RPBs is in steady-state.

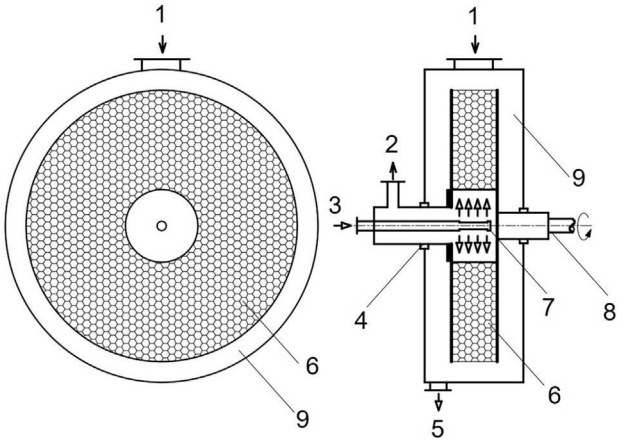

Fig. 1. Schematic diagram of a typical rotating packed bed (1. Gas inlet; 2. Gas outlet; 3. Liquid inlet; 4. Seal; 5. Liquid outlet; 6. Packing; 7. Liquid distributor; 8. Rotating shaft; 9. Static chamber).

Thus, a very promising method to resolve these problems is a porous media model with an Eulerian method because of the lower requirement for the number of the meshes and the shorter simulation times. For the Euler-Euler method, the porous media model consists of the drag force between the gas and liquid, the gas and solids and the liquid and solids. For CFD simulations of gas-liquid two-phase flows in packed beds or trickle beds, the available porous media models are the Attou, Lappalainen and Iliuta models (Attou et al., 1999; Lappalainen et al., 2008; Iliuta et al., 2004). In addition to these models, the Zhang model (Zhang and Bokil, 1997) may be used for the wire screen packing or tube bundle packing for demisting or condensation. Schematic diagrams of these models are presented in Fig. 2.

The Attou model (Attou et al., 1999) assumes a smooth liquid film flow on the packed spheres, the gas flowing through the empty space in the packing area and the gas separated from the liquid by a stable interface. Thus, the interaction between each phase pair is described by the one-phase Kozeny-Carman equation. Finally, the form of each equation for the interaction between the gas-liquid, liquid-solids and gas-solids is similar to the Ergun equation. This model is widely accepted and used in CFD simulations of traditional packed beds (Lopes and Quinta-Ferreira, 2009; Solomenko et al., 2015; Jindal and Buwa, 2017). Lappalainen et al. (2008, 2009) constructed a porous media model based on the wetting efficiency and packing of spheres. The total interaction force for the gas and liquid is the drag force between the gas and liquid minus the interaction force between the solids and liquid or gas. For the gas-liquid drag force and the interaction force between the solids and liquid or gas, the form of the Ergun equation is also used. Heidari et al. (2014) combined the Lappalainen model and the Attou model in their simulations. Both the Attou and Lappalainen models assume that the packing materials are ideal spheres and the liquid flows as a film on the surface of the spheres. In addition, the Attou model assumes that a liquid film covers the solid spheres and the gas flow does not exert a direct action on the packing surface. While, in the Lappalainen model, it is assumed that part of the surface of the spheres is covered by the liquid and thus introduces the wettability, f_e, namely the packing wetted area fraction to the total packing area.

Iliuta et al. (2004) developed a porous media model for the structured packing containing columns. They treated the flow structure as a simplified two-parallel interconnected inclined slits, a dry slit $a_S \times (1 - f_e)$ and a gas-liquid wet slit $a_S \times f_e$ with the liquid film on the slit surface and the gas does not directly act on the solids slit. The shear stresses exerted by the slit wall are assumed to be composed of laminar and turbulent contributions. The partial wetting gas-phase drag force consists of gas-liquid and gas-solids interactions and the particle plus wetting liquid phase drag force, which consists of gas-liquid and liquid-solids interactions. The pressure drop across the dry slit is equal to the pressure drop across the wet slit. In addition, this model is popular in CFD simulations for a structured packing bed (Pham et al., 2015; Fourati et al., 2013). The Iliuta model is specifically designed for the structure slit packing.

Zhang and Bokil (1997) built a resistance model for tube bundle condensers and Al-Fulaij et al. (2014) used this model for the Euler-Euler simulation of wire mesh demisters and treated the demister wires as the porous media. This model assumes that the liquid exists as droplets of a single size in the middle of the tube and as a film on the tube wall. The drag forces between the gas and solids or between the liquid and the solids are the friction between the two phases. In the Zhang and Bokil model (Zhang and Bokil, 1997), the interaction force is attributed to the friction between the interfaces.

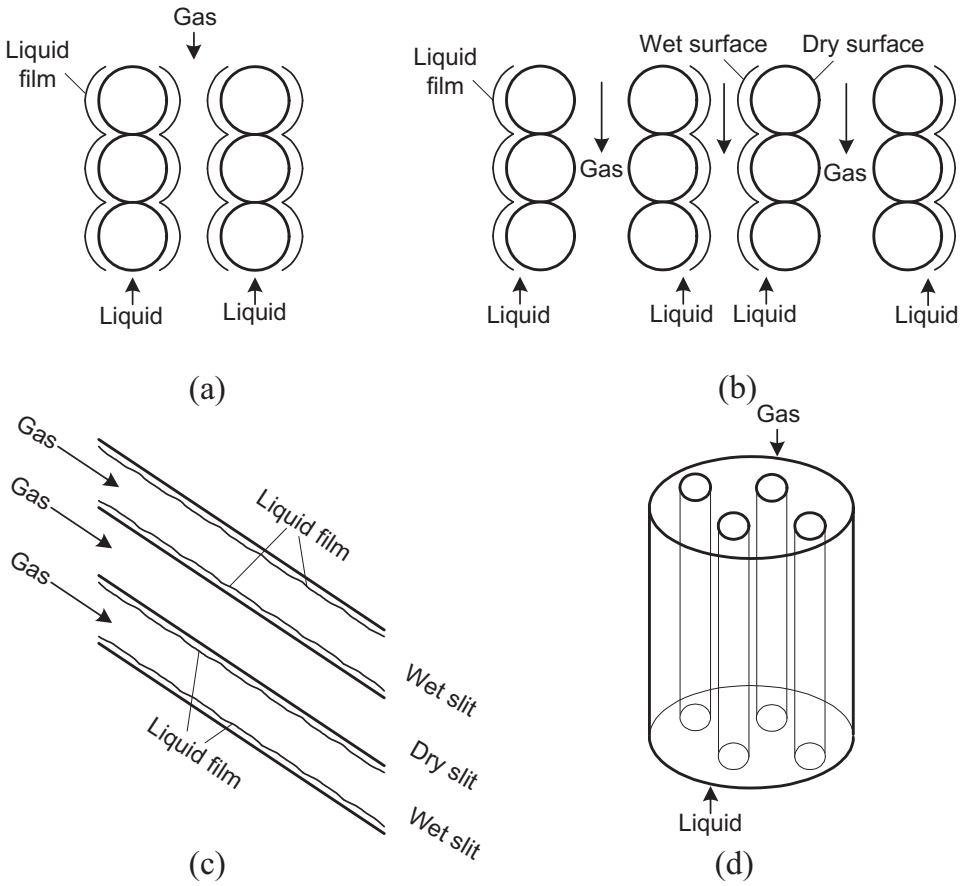

Fig. 2. Schematic diagram of the porous media models (a) Attou, (b) Lappalainen, (c) Iliuta and (d) Zhang.

These porous media models are effective to be applied for traditional packed beds. However, these models are not suitable for the RPB. The reasons are (i) the packing materials are different. For the RPBs, the high porosity wire screens are commonly used as the packing materials, but for traditional packed beds, the spheres or spherical patterns are commonly used; (ii) the packing structurers are different. The basic structure of wire screens are cylinders. Therefore, the hydraulic diameter should be cylinder diameter. For the traditional packed beds, the hydraulic diameter is the sphere diameter; and (iii) the flow characteristics are different. Kołodziej and Łojewska (2009) investigated one-phase flow through wire screens and analysed the pressure drop through the Fanning factor. They found that the flow through the wire mesh is different from what occurs in traditional packing. Therefore, these existing porous media models cannot be used for RPBs.

Therefore, the purpose of this paper is to construct a new porous media model for CFD simulations of gas-liquid two-phase flows in RPBs and to obtain reasonable and accurate liquid holdup distributions.

2. Simulations

2.1. Gas-liquid two-phase porous media model

In most situations, the packing materials in RPBs are the stacked wire screens and the characteristics of this type of packing for two-phase flows are different from sphere packing used in the traditional packed beds. In general, the traditional Ergun equation cannot predict the correct flow hydrodynamics in wire screen packed beds. Kołodziej et al. (2009) compared different one-phase porous media models and built a new one-phase model for wire screen packing. The model combines two equations: the Blake-Kozeny's equation for the laminar flow pressure drop and the Burke-Plummer's equation for the turbulent flow pressure drop. Finally, the model equation is modified to the analogical form of the Ergun equation. The model equation (Kołodziej et al., 2009) is given by

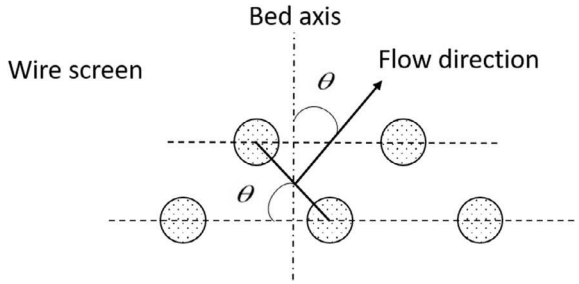

Fig. 3. Angle of slope, θ (Kołodziej et al., 2009).

$$\frac{\Delta P}{H} = 4(f_{app} + f_t)\frac{\rho v^2}{2d_w}\frac{(1-\varepsilon)}{\varepsilon^3}\frac{\tau^3}{\cos^3(\theta)} \quad (1)$$

where ΔP is the pressure drop; H is the height of the packed bed; f_{app} is the Fanning friction factor for laminar flows; f_t is the Fanning friction factor for turbulence flow; ρ is the fluid density; v is the fluid velocity; d_w is the diameter of the packed wires; ε is the porosity of the packed bed; τ is the bed tortuosity factor; θ is the angle between flow direction and the bed axis as shown in Fig. 3.

In this work, we develop a new two-phase porous media model for a wire screen packing based on the Kołodziej one-phase model.

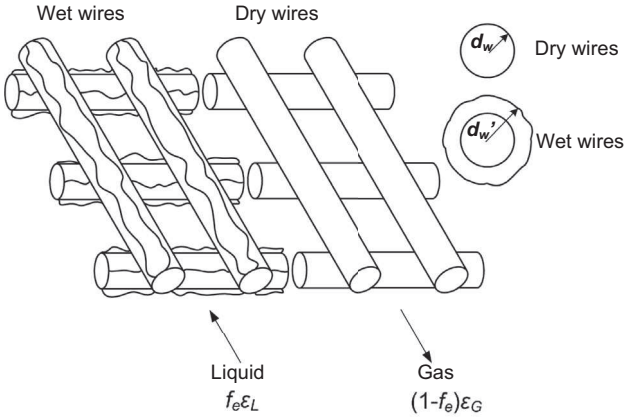

Fig. 4. Schematic diagram of the porous media model based on wet wires and dry wires.

The new model is suitable for wire-like packed beds with high porosity. The basic assumptions are as shown in Fig. 4: (i) part of the wires, called wet wires, f_e, are covered by liquid and the remaining wires, called dry wires, (1 - f_e), are directly in contacted with the gas. In the concept of the porous media model, the packings are modelled as a homogenous porous medium without resolving the detailed packing structures in the computational mesh. Therefore, the wetted part of the specific single wire is considered using the local averaged values of the wetting fraction; (ii) there are three interactions: liquid flowing on the wet wire surface which is controlled by the interaction force between the liquid and solids, gas flowing on the dry wire surface which is controlled by the interaction drag force between the gas and solids and the gas flowing through the surface of the liquid on the wet wires which is controlled by the interaction drag force between the gas and liquid; (iii) when the gas and liquid flows through the wire screen, the pressure drop across the wet surface is equal to the pressure drop across the dry surface; (iv) the gas and liquid flow through the packing wire screens follow the physics of the Kołodziej one-phase flow porous media equation (Kołodziej and Łojewska, 2009); and (v) for the interaction drag force between the gas and liquid, the wire size considers the enlargement, d_w' instead of d_w, caused by the liquid film, and the gas-liquid drag force follows the Kołodziej equations with $\theta = 0°$, which means the gas and liquid flows in the opposite direction but on the same line.

The total interactions for the gas and liquid phase are given, respectively, by

$$F_{int,G} = -f_e F_{GL} - (1 - f_e) F_{GS} \tag{2}$$

$$F_{int,L} = f_e (F_{GL} - F_{LS}) \tag{3}$$

where $F_{int,G}$ and $F_{int,L}$ are the total interaction force for the gas phase or liquid phase; f_e is the wetted fraction of the packing bed; F_{GL}, F_{GS} and F_{LS} are the drag forces between the gas and the liquid, the gas and the solids and the liquid and the solids.

Therefore, the equations for the new model employed are as follows:

$$F_{LS} = f_e \varepsilon_L \left[4(f_{app} + f_t) \frac{\rho_L v_L^2}{2 d_w} \frac{\varepsilon_S}{\varepsilon_L^3} \frac{\tau^3}{\cos^3 \theta} \right] \tag{4}$$

$$F_{GS} = (1 - f_e) \varepsilon_G \left[4(f_{app} + f_t) \frac{\rho_G v_G^2}{2 d_w} \frac{(1 - \varepsilon_G)}{\varepsilon_G^3} \frac{\tau^3}{\cos^3 \theta} \right] \tag{5}$$

$$F_{GL} = f_e \varepsilon_G \left[4(f_{app} + f_t) \frac{\rho_G (v_G - v_L)^2}{2 d_w'} \frac{(1 - \varepsilon_G)}{\varepsilon_G^3} \frac{\tau^3}{\cos^3 \theta} \right] \tag{6}$$

where, ε_G, ε_L and ε_S are the volume fraction of the gas, liquid or the solid phase; d'_w is the diameter of the wetted wires.

The Fanning friction factor for laminar flows, f_{app}, is given by (Kołodziej and Łojewska, 2009):

$$f_{app} = \frac{1}{Re_K} \left(\frac{3.44}{\sqrt{\chi^+}} + \frac{\frac{1.25}{4\chi^+} + 16 - \frac{3.44}{\sqrt{\chi^+}}}{1 + \frac{0.00021}{\chi^{+2}}} \right) \tag{7}$$

The Fanning friction factor for turbulence flows, f_t, is given by Kołodziej and Łojewska (2009):

$$f_t = \frac{0.079}{Re_K^{0.25}} \tag{8}$$

$$\chi^+ = \frac{d_w}{D_h Re_K} \tag{9}$$

$$Re_K = \frac{\rho v_e D_h}{\mu} \tag{10}$$

where χ^+ is dimensionless channel length; Re_K is the Reynold number in the Kołodziej model; v_e is the effective velocity; D_h is the hydraulic diameter of the packed bed; μ is the viscosity of the fluid.

For gas-solids interaction:

$$\tau = 1 + \frac{\varepsilon_S}{2}, \quad d_w = \frac{4\varepsilon_S}{a_S}, \quad v_e = \frac{v}{\varepsilon_G} \frac{\tau}{\cos(\theta)}, \quad D_h = \frac{4\varepsilon_G}{a_S} \tag{11}$$

For liquid-solids interaction:

$$\tau = 1 + \frac{\varepsilon_S}{2}, \quad d_w = \frac{4\varepsilon_S}{a_S}, \quad v_e = \frac{v}{\varepsilon_L} \frac{\tau}{\cos(\theta)}, \quad D_h = \frac{4\varepsilon_L}{a_S} \tag{12}$$

For gas-liquid interaction:

$$\tau = 1 + \frac{\varepsilon_S + \varepsilon_L}{2}, \quad d'_w = \frac{4\varepsilon_S}{a'_S}, \quad v_e = \frac{v\tau}{\varepsilon_G}, \quad D_h = \frac{4\varepsilon_G}{a'_S} \tag{13}$$

$$a'_S = \left(\frac{\varepsilon_L + \varepsilon_S}{\varepsilon_S} \right)^{\frac{1}{2}} a_S \tag{14}$$

where a'_S is the specific area of the wetted wires. For the gas-liquid interaction, the gas and liquid flow are assumed to be $\theta = 0°$.

The wetted surface fraction, f_e, is calculated from the Onda correlation (Onda et al., 1968) and it is given as follows:

$$f_e = 1 - exp\left[-1.45 \left(\frac{\sigma_c}{\sigma} \right)^{0.75} Re_L^{0.1} We_L^{0.2} Fr_L^{-0.05} \right] \tag{15}$$

$Re_L = \frac{\rho_L v_L}{a_S \mu_L}$, $We_L = \frac{v_L^2 \rho_L}{a_S \sigma}$, $Fr_L = \frac{v_L^2 a_S}{g_c}$, $g_c = r\omega^2$. where, Re_L is the Reynold number of the liquid phase; We_L is the Webber number of the liquid phase; Fr_L is the Froude number of the liquid phase; σ is the surface tension; σ_c is the critical surface tension; g_c is the centrifugal acceleration; r is the radius of the rotation; ω is the rotation speed.

In reality, the liquid film and liquid droplets all exist in the RPB. However, the motion of the liquid droplets in the RPB are restricted by the packing mesh and they interact with the film flow. Currently, it is still difficult to determine the volume ratio of the liquid droplets to the liquid film in an RPB. Although the gas-liquid two-phase porous media model in this work is derived from the liquid film flow, we will explore the capability of this model for simulating the flow containing droplets. This concept is also used by CFD simulations of traditional trickle beds (Gunjal et al., 2005; Lopes and Quinta-Ferreira, 2008).

2.2. Simulation cases

In order to validate the simulation, two experimental cases with high porosity packing from the literatures are used, namely the

Table 1
Simulation cases: dimensions and packing materials.

Case authors	Dimensions			Packing		
	Inner radius (mm)	Outer radius (mm)	Thickness (mm)	Materials	Voidage	Specific area (m^2/m^3)
Burns et al. (2000)	35	160	10	Foams with interconnected filaments	0.953	786
Yang et al. (2015)	21	41	20	Wire mesh	0.95	497

Burns experiment (Burns et al., 2000) on the gas-liquid counter-current flow in a RPB and the experiments of Yang et al. (2015) in a RPB. These two experiments are the representative type experiments in measuring liquid holdup in the RPB. The Burns correlation for liquid holdup, which was obtained from the experimental data, has been examined, accepted and extensively applied by many other researchers (Kang et al., 2014; Joel et al., 2014). In the Yang experiment, the advanced non-invasive X-ray CT, IPECT160, which was developed by the State Key Laboratory of Multi-phase Complex System of China (Yang et al., 2015), was employed to measure the liquid holdup distribution. The experimental data for liquid holdup from the Yang experiment are often used to validate the CFD simulation of liquid flow in RPBs (Xie et al., 2017; Ouyang et al., 2018). Therefore, the experimental data from these two experiments were chosen to be used as the validation data in this work. The dimensions of the RPBs and the packing materials are listed in Table 1.

The prediction of the liquid holdup for two-phase flow in packed beds is of great importance in industrial processes (Saez and Carbonell, 1985). The validation of the simulation presented in this work is performed by comparison of the liquid holdup between the simulations and the experimental data.

The Burns experimental correlation for the liquid holdup is given by

$$h_L = 0.039\left(\frac{g_c}{g_0}\right)^{-0.5}\left(\frac{U}{U_0}\right)^{0.6}\left(\frac{\nu}{\nu_0}\right)^{0.22} \tag{16}$$

where $g_0 = 100\ m\ s^{-2}$, $U_0 = 0.01\ m\ s^{-1}$ and $\nu_0 = 1\ cS$; h_L is the liquid holdup; U is the superficial velocity; ν is the kinematic viscosity.

The Yang experimental results for the liquid holdup are shown in Fig. 9 in their paper (Yang et al., 2015).

2.3. Simulation method

The gas-liquid two-phase flow in a rotating packed bed is almost axisymmetric and this has been demonstrated in the literature (Yang et al., 2015). Therefore, for simplifying the simulation without compromising the integrity of the flow characteristics in this paper, a 2D axisymmetric laminar flow model is used for the CFD simulations of the RPBs, in which the gas and liquid flows in the RPB are counter-current flows. In addition, the rotation of the bed is considered using the rotating reference frame with an appropriate rotating speed. The further assumptions made are as follows: (i) the porous media is isotropic; (ii) the liquid flow in the RPBs is steady-state; (iii) the gas is incompressible; (iv) the liquid is treated to be a uniform flow entering the packed bed; The liquid entry region and the effect of the liquid jet on the liquid flowing in the packed bed are not considered; (v) the liquid flow in the packed bed is dominated by the form of the film and the dispersed droplets; and (vi) the flow between two plates in the packed bed is symmetrically distributed on both sides of the midline.

A schematic diagram of the 2D RPB model is shown in Fig. 5. On left side of the bed is a no slip wall and on the right side is a symmetry boundary. The top outer boundary is the gas velocity inlet and the bottom inner boundary is a gas pressure outlet. The simulation for the counter-current flow in the rotating packed bed is

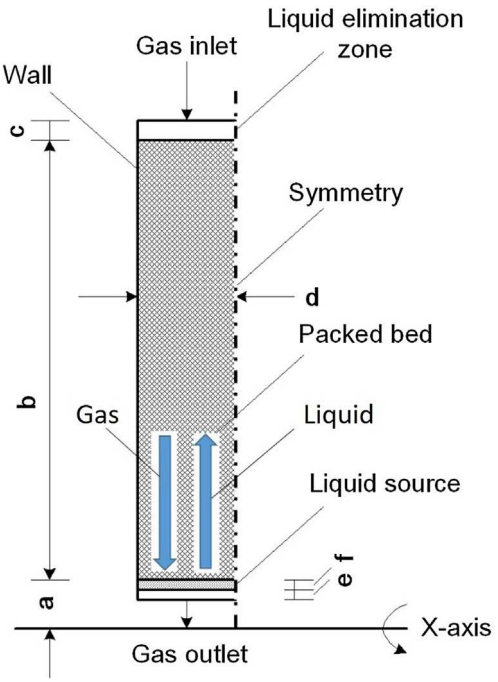

Fig. 5. Schematic diagram of the 2D model (a, b, c, d, e and f stand for the length of the corresponding sections in the figure).

challenging due to the difficulty in the accurately setting of the liquid inlet and liquid outlet. This is because the liquid inlet and the gas outlet are overlapping, and the liquid outlet and the gas inlet are overlapping. There is no accurate available boundary settings for them in FLUENT and therefore in order to overcome this difficulty, two zones, namely a liquid source zone and a liquid elimination zone, were constructed. The liquid is generated from the liquid source zone, in which the mass source is added, and the flow is towards the outer boundary, and it finally disappears in the liquid elimination zone in which the liquid mass and momentum are extracted. The gas outlet of the RPB is at a certain distance away from the x-axis and rotates about the x-axis. The detailed dimensions and properties of the materials are listed in Table 2.

The governing equations, closure model equations are as follows:

(i) Mass equation:

$$\frac{\partial}{\partial x}(\rho_i\alpha_i v_{x,i}) + \frac{\partial}{\partial r}(\rho_i\alpha_i v_{r,i}) + \frac{\rho_i\alpha_i v_{r,i}}{r} = S_{m,i} \tag{17}$$

$$\alpha_L + \alpha_G = 1 \tag{18}$$

(ii) Momentum equation

Axial direction:

$$\frac{1}{r}\frac{\partial}{\partial x}(r\rho_i\alpha_i v_{x,i}v_{x,i}) + \frac{1}{r}\frac{\partial}{\partial r}(r\rho_i\alpha_i v_{r,i}v_{x,i}) = -\frac{\partial P}{\partial x} + \frac{1}{r}\frac{\partial}{\partial x}\left[r\mu_i\left(2\frac{\partial v_{x,i}}{\partial x}\right)\right] + \frac{1}{r}\frac{\partial}{\partial r}\left[r\mu_i\left(\frac{\partial v_{x,i}}{\partial r} + \frac{\partial v_{r,i}}{\partial x}\right)\right] + F_{drag,x} - S_{x,i} \tag{19}$$

Table 2
Dimensions of the simulation physical model and physical properties of the materials.

Dimension	Burns et al. (2000)	Yang et al. (2015)	Materials Gas: air	
a, mm	35	21	Density, kg/m^3	1.225
b, mm	125	20	Viscosity, Pa s	1.7894×10^{-5}
c, mm	2	1	Liquid: water	
d, mm	5	10	Density, kg/m^3	998.2
e, mm	2	1.5	Viscosity, Pa s	0.001003
f, mm	1	0.5		
Mesh	30×500	40×80		

Radial direction:

$$\frac{1}{r}\frac{\partial}{\partial x}(r\rho_i\alpha_i v_{x,i}v_{r,i}) + \frac{1}{r}\frac{\partial}{\partial r}(r\rho_i\alpha_i v_{r,i}v_{r,i}) = -\frac{\partial P}{\partial r} + \frac{1}{r}\frac{\partial}{\partial x}\left[r\mu_i\left(\frac{\partial v_{r,i}}{\partial x} + \frac{\partial v_{x,i}}{\partial r}\right)\right] + \frac{1}{r}\frac{\partial}{\partial r}\left[r\mu_i\left(2\frac{\partial v_{r,i}}{\partial r}\right)\right] - 2\mu_i\frac{v_{r,i}}{r^2} + \rho_i\alpha_i\frac{v_{z,i}^2}{r} + F_{drag,r} - S_{r,i} \quad (20)$$

• Tangential direction:

$$\frac{1}{r}\frac{\partial}{\partial x}(r\rho_i\alpha_i v_{r,i}v_{z,i}) + \frac{1}{r}\frac{\partial}{\partial r}(r\rho_i\alpha_i v_{x,i}v_{z,i}) = \frac{1}{r}\frac{\partial}{\partial x}\left[r\mu_i\frac{\partial v_{z,i}}{\partial x}\right] + \frac{1}{r^2}\frac{\partial}{\partial}\left[r^3\mu_i\frac{\partial}{\partial r}\left(\frac{v_{z,i}}{r}\right)\right] - \rho_i\alpha_i\frac{v_{x,i}v_{z,i}}{r} + F_{drag,z} - S_{z,i} \quad (21)$$

(iii) Liquid source zone:
For the liquid mass source,

$$S_{m,L} = \frac{Q_L\rho_L}{\pi(r_2^2 - r_1^2)h} \quad (22)$$

(iv) Liquid elimination zone:
For the liquid mass source,

$$S_{m,L} = -\left(\frac{\rho_L\alpha_L v_{x,L}}{\Delta x} + \frac{\rho_L\alpha_L v_{r,L}}{\Delta r} + \frac{\rho_L\alpha_L v_{r,L}}{r}\right) \quad (23)$$

For the liquid momentum source,

$$S_{x,L} = -\left(\frac{1}{r}\frac{r\rho_L\alpha_L v_{x,L}v_{x,L}}{\Delta x} + \frac{1}{r}\frac{r\rho_L\alpha_L v_{r,L}v_{x,L}}{\Delta r}\right) \quad (24)$$

$$S_{r,L} = -\left(\frac{1}{r}\frac{r\rho_L\alpha_L v_{x,L}v_{r,L}}{\Delta x} + \frac{1}{r}\frac{r\rho_L\alpha_L v_{r,L}v_{r,L}}{\Delta r}\right) \quad (25)$$

$$S_{z,L} = -\left(\frac{1}{r}\frac{r\rho_L\alpha_L v_{r,L}v_{z,L}}{\Delta x} + \frac{1}{r}\frac{r\rho_L\alpha_L v_{x,L}v_{z,L}}{\Delta r}\right) \quad (26)$$

where x, r and z are the axial, radial and tangential coordinate, respectively; i stands for the gas phase or liquid phase; α_L and α_G are the phase fraction for the liquid and gas phase, respectively; S_m is the mass source; S_x, S_r and S_z are the momentum sources in the axial, radial and tangential directions, respectively; F_{drag} is the drag force; Q_L is the volume flow rate of the liquid; h is the thickness of the RPB.

(v) Porous media model (interaction force between the gas and solids, interaction force between the liquid and solids):

$$S_i = -\left(\frac{\mu}{\alpha_1}v_i + C_2\frac{1}{2}\rho_i|v_i|v_i\right) \quad (27)$$

where, α_1 is the viscous resistance coefficient in porous media; C_2 is the inertial resistance coefficient in porous media.

(vi) Drag force model (interaction force between gas and liquid):

$$F_{drag} = F'_{GL}(v_G - v_L) \quad (28)$$

where F'_{GL} is the interphase momentum exchange coefficient.

For the solver, the pressure based method and the relative velocity formulation are used. During the simulation, the COUPLE method is employed. The second-order upwind discretisation schemes are used for the momentum equation and the swirl velocity equation, and the QUICK scheme is used for the volume fraction equation. The convergent condition is that the continuity residual is less than 1×10^{-3} and reaches a constant value; the residuals in the liquid and gas velocities are less than 1×10^{-4} and all reach a constant value; the liquid holdup does not change with increasing iterations. The mesh independence is checked and the simulation software is Fluent 16.1.0. The porous media models are implemented by UDF source codes in Fluent. The 2D simulations are used on a PC with parallel computing facilities based on 10 processes and double precision.

3. Results and discussion

3.1. Validation of the new model and the effect of flow angle on the liquid holdup distribution

In the new porous media model, there is a key parameter, θ, which is the angle of the flow direction to the axis of the bed and it combines the tortuosity factor τ to take into account the extended flow length. The value of θ is determined by the packing structures and the flow characteristics as shown in Fig. 3. Bussière et al. (2017) obtained θ through a pressure drop testing and Eq. (1). Because of the complexity in the stack screen packing, it is difficult to achieve θ directly in this work but it can be obtained through an indirect method, which is through the validation of the simulation with the experimental data on the liquid holdup distributions.

To demonstrate the effectiveness of the new model and obtain θ for predicting the liquid flow in the RPB, two experimental cases, namely the Burns and Yang experimental data are used.

For the Burns experiment, the operation conditions are Q_L = 17.5 cm^3/s, Q_G = 2.0 cm^3/s and n = 600 rpm. Because the experimental correlation equation proposed by Burns et al. (2000) is used for validation, the experimental data from the correlation all lie on a smooth curve. The simulation results and experimental results are presented in Fig. 6(a). For the Yang experiment, the operating conditions are Q_L = 22.9 cm^3/s and n = 1500 rpm. In the experiment of Yang, no gas is input into the rig but in the simulation, a small gas flow is added into the rig in order to obtain a rapid convergence but this small gas flow does not influence the liquid holdup and this was demonstrated by Burns et al. (2000). The gas velocity is set as 0.01 m s^{-1}. The simulation results are compared with the liquid holdup experimental data (Yang et al., 2015) and these are shown in Fig. 6(b). In the experiment of Yang, the liquid flow in the RPB can be divided into three regions (Yang et al., 2015): namely the entrance, bulk and near wall regions. At the entrance region, the liquid holdup along the radial direction increases from the inner edge of the RPB to the boundary of the bulk region. In the bulk region, the liquid holdup decreases with the radial direction and in the wall region, the liquid holdup increases up to the outer

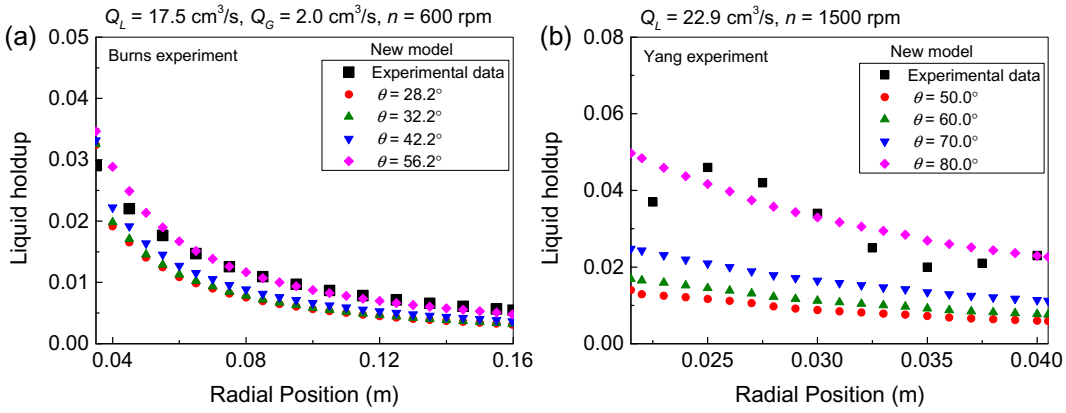

Fig. 6. The liquid holdup as a function of radial position for the new proposed model for the experimental data of (a) Burns et al. (2000), and (b) Yang et al. (2015), under different values of θ.

edge of the RPB. The experimental data that is employed for validation does not vary in a smooth manner and this is because of the manner of the liquid-inlet water spraying and the limitation of the liquid-outlet shell. For the CFD simulations in this work, the entrance and near wall regions are not modelled exactly, namely (i) the liquid inlet is treated as a liquid uniformly flowing into the RPB and the effect of the water jet is not considered; and (ii) the liquid outlet is treated as a liquid that disappears naturally when all the liquid is flowing out of the RPB.

For the simulation of these two experimental cases, it can be observed from Fig. 6 that there are two similarities: (i) at a specific value of θ, for these two experimental cases, the predicted liquid holdup is very close to the experimental correlation values. For example, for the Burns experiment, the error at the outer boundary of the RPB is 12.6% at θ = 56.2°; for the Yang experiment, the error is 1.6% at θ = 80.0°, and (ii) with increasingθ, the predicted liquid holdup increases correspondingly. For the Burns experiment, as θ increases from 28.2° to 56.2°, the liquid holdup at the outer boundary of the RPB is enhanced from 0.003 to 0.005. For the Yang experiment, when θ increases from 50.0° to 80.0°, the liquid holdup at the outer boundary of the RPB is enhanced from 0.006 to 0.023. An increase in θ results in an increase in the flow resistance because a higher θ means that the gas or liquid flow is twisted more heavily and extends much longer into the porous media.

Attention in the simulations to these cases should be paid to the validation and the values of θ that are different for different experiments and they are 56.2° and 80.0° for the Burns and Yang experiments, respectively. Bussière et al. (2017) investigated the one-phase flow in woven metal mesh screens and obtained θ in the range of 79.4° - 85.5° for packings with different mesh size, warp wire diameter, weft wire diameter and single screen thickness. Therefore, it can be seen that θ is one of the characteristics of the packing and different packing materials have their own specified value of θ. It is a function of the packing structure and flow direction and does not vary with other flow parameters, such as liquid or gas flow rate, rotation speed, etc.

3.2. Effect of the rotating speed on the liquid holdup distribution

In order to assess the new model further, different rotating speeds are used for examining the effectiveness of the new model with θ = 56.2° or 80.0°, respectively, for the Burns and Yang experimental data.

Based on the Burns experiment, simulations were carried out with the rotation speeds 600 rpm, 917 rpm and 1200 rpm and the results obtained are shown in Fig. 7(a). At the entrance region (r < 50 mm), the liquid holdups are estimated to be 20% higher than the experimental values under different rotation speeds. This may be caused by the liquid inlet, which is not modelled exactly. In other regions, the liquid holdup distribution is almost the same as the experimental data and the error is within 13%.

In the experimental work performed by Yang et al. (2015), the rotation speeds were 1000 rpm, 1500 rpm and 2500 rpm and these values were employed in the present simulation. Fig. 7(b) shows that for rotational speeds 1500 rpm and 2500 rpm, the simulated liquid holdup distributions agree well with the experimental data. The error for the liquid holdup at the outer boundary of the RPB is 13%. In the wall region (r = ~35–41 mm), the liquid holdup is predicted to be lower than the experimental data. For the rotation speed of 1000 rpm, the predicted difference for the liquid holdup at the outer boundary of the RPB is about 30%. The reason may be that the Yang experiment was affected by the liquid entry and exit wall region (Yang et al., 2015) whereas the simulation treated the liquid inlet and outlet without including the wall effect.

The above simulation results demonstrate, at different rotating speeds, that the new porous media model is effective in describing the liquid flow in the RPB.

3.3. Effect of liquid flow rate on the liquid holdup distribution

In this section, the simulation with the new model is tested under different liquid flow rates and θ = 56.2° and 80.0° are still employed for the Burns and Yang experimental data, respectively.

Fig. 8(a) shows a comparison between the predicted liquid holdup distribution and the Burns experimental data under different liquid flow rates, namely 9.0 cm³/s, 17.5 cm³/s and 35.0 cm³/s. The results obtained indicate that the simulated results approach the experimental results in most of the region (r = ~60–160 mm), with the errors being within 15%, and at the liquid entrance region the simulation obtained values that are slightly larger than the experimental data. In Fig. 8(a), near the inner boundary of the RPB, the liquid holdup in the experimental work of Burns shows a smooth decrease along the radial direction of the RPB. This is because the experimental data is obtained from a correlation equation. Fig. 8(b) shows the simulation results under the Yang experimental conditions with two different liquid flow rates, namely 22.9 cm³/s and 43.0 cm³/s and it is observed that the predicted liquid holdup results agree well with the experimental data. For 22.9 cm³/s and 43.0 cm³/s, the liquid holdups at the outer boundary of the RPB from the experiment are 0.023 and 0.038, respectively and the corresponding liquid holdups from the simulation are 0.023 and 0.037, respectively. Thus, the error is within 10%. Fig. 8(b) shows the liquid holdup near the inner boundary of the RPB, as obtained experimentally, first the liquid holdup increases sharply

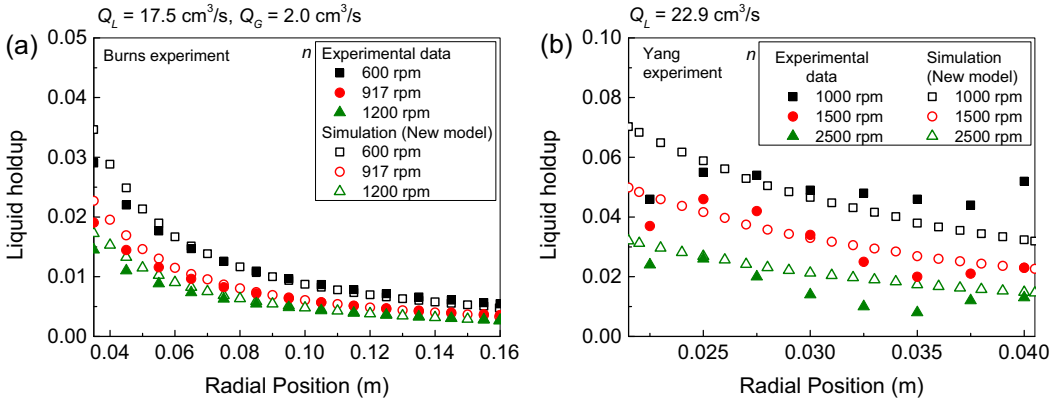

Fig. 7. The liquid holdup as a function of radial position for the different porous media models for the experimental data of (a) Burns et al. (2000), and (b) Yang et al. (2015), under different rotation speeds.

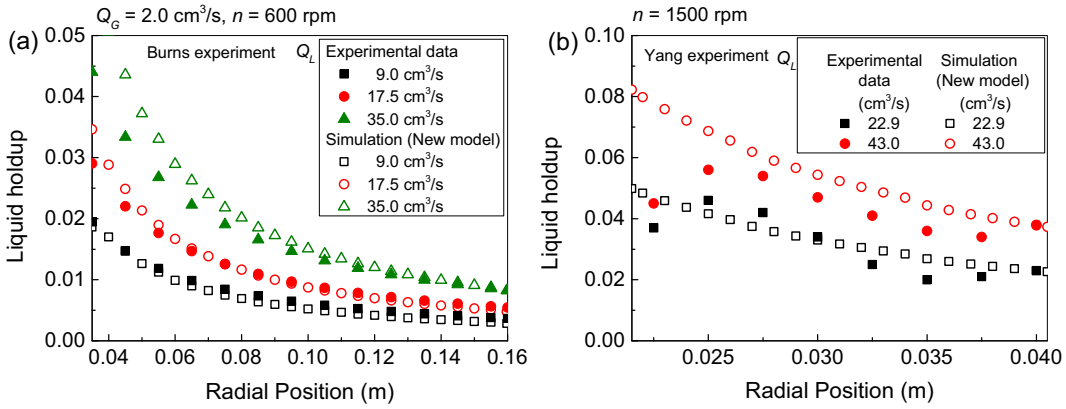

Fig. 8. The liquid holdup as a function of radial position for the different porous media models for the experimental data of (a) Burns et al. (2000), and (b) Yang et al. (2015), under different liquid flow rates.

and then decreases slowly, but the simulations show a smooth curve with the liquid holdup decreasing along the radial direction of the RPB. The reason for this behaviour is that this experimental data is affected by the liquid inlet, however, the simulations do not take into account the effect of the liquid jetting on the inner boundary of the RPB as mentioned earlier.

Fig. 8 illustrates that the new porous media model, under different liquid flow rates, is still effective for describing the liquid flow in the RPB. Due to being derived from the Kołodziej wire mesh model, the new two-phase porous media model is suitable for high-porosity stacked wire mesh packing.

3.4. Pressure drop

The pressure drop is also an important quantity when evaluating porous media models. Here, the pressure drop data from the simulation based on the Burns experiments are presented in Fig. 9. It is found that the gas volume flow rate is 2.0 cm^3/s and the gas radial velocity at the inner boundary of the packed bed is 0.91 m/s, and the simulated pressure drops are 139 Pa, 216 Pa and 319 Pa for the rotation speeds 600 rpm, 917 rpm and 1200 rpm, respectively. Because the Burns experiment did not give the experimental data for the pressure drop, then the pressure drop cannot be validated directly. However, we can compare this pressure drop data with those obtained under similar experimental conditions in order to check if it is reasonable. For example, in the Hassan-Beck experiment (Hassan-Beck, 1997), the dimensions of the packed bed has an inner diameter 79 mm, outer diameter

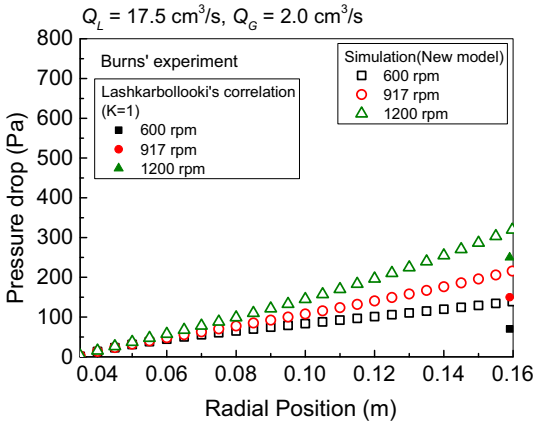

Fig. 9. The pressure drop as a function of radial position for the new proposed model for the experimental data of Burns et al. (2000) under different rotation speeds.

201 mm and thickness 60 mm. The properties of the packing materials have a porosity 0.83 and specific area 1428 m^2/m^3; the operation conditions are Q_L = 10.5 L/min or 14.4 L/min, Q_G = 50–70 m^3/h and n = 620 rpm; and the pressure drop is 20–50 mmH_2O (196–490 Pa). Another example is the Liu et al. (2017) experiment and in this case, the dimension of the packed bed has an inner diameter 72.5 mm, outer diameter 160 mm and thickness 55 mm; the properties of the packing materials are that the porosity is 0.94 and a

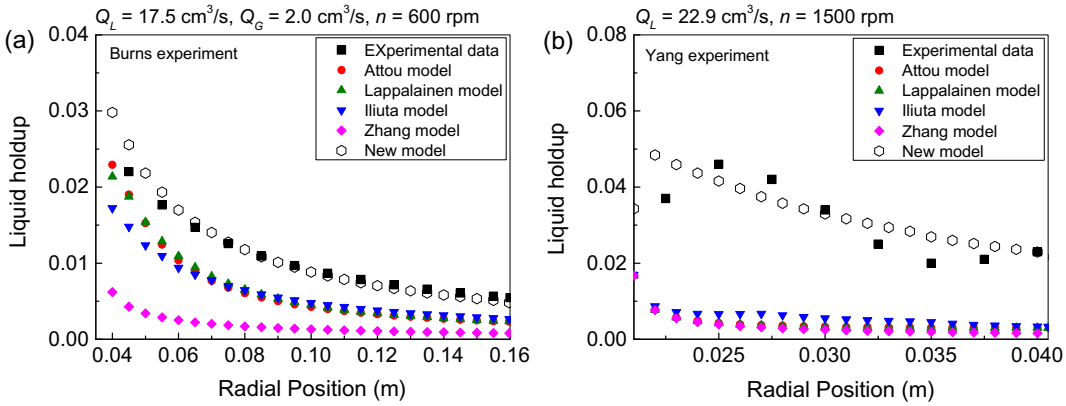

Fig. 10. The liquid holdup as a function of radial position for the different porous media models for the experimental data of (a) Burns et al. (2000), and (b) Yang et al. (2015).

specific area 385 m^2/m^3. Under the condition of Q_G = 10 m^3/h and n = 400 rpm, the pressure drop is 50 Pa; under Q_G = 10 m^3/h and n = 1000 rpm, the pressure drop is 300 Pa. From a similar experiment on the gas flow rate, liquid flow rate and rotation speed, the simulated pressure is reasonable and all values are in the range of 100–400 Pa.

Lashkarbolooki (2017) built a general model to predict the pressure drop in a gas-liquid counter-current two-phase flow across rotating packed beds. The model includes three parts: part I, the drag force pressure drop; Part II, the rotational pressure drop; and Part III, the slip pressure drop, as follows:

$$\Delta P_I = A\left(\frac{GFR}{2\pi h}\right) ln\left(\frac{r_o}{r_i}\right) + B\left(\frac{GFR}{2\pi h}\right)^2 \left(\frac{1}{r_i} - \frac{1}{r_o}\right) \tag{29}$$

$$\Delta P_{II} = \frac{1}{2}\rho_G (K\omega)^2 (r_o^2 - r_i^2) \tag{30}$$

$$\Delta P_{III} = (\beta_1 + \beta_2)(v_G - v_L) \tag{31}$$

where A and B are the constants of the viscous and inertial terms in Eq. (29), respectively; K is the wall factor in Eq. (30); β_1 and β_2 are the gas-packing and gas-liquid slip parameters in Eq. (31), respectively.

The estimated total pressure drop from these equations for the Burns experiment is 70 Pa, 150 Pa and 250 Pa for the rotation speeds n = 600, 917, 1200 rpm, respectively. Here, K in Eq. (30) accounts for the end effect due to the pressure measurement not being exactly at the inner and outer radius of the rotating packed bed and it is taken as 1 in this work since the rig is small and a small gas flow rate is used. The values of A, B, β_1 and β_2 in Eqs. (29)–(31) are all estimated from correlations in the literature (Lashkarbolooki, 2017). The Lashkarbolooki equations may under-estimate the pressure drop for the Burns experimental case because ΔP_I, the drag force pressure drop from Eq. (29), is estimated to be 0.0012 Pa, which means that the friction between the fluid and the packing is nearly to be 0. It does not conform to reality.

From the other experiments mentioned above and the Lashkarbolooki correlation, it is concluded that the CFD predicted pressure drop with the new proposed porous media model is reasonable.

3.5. Comparison of new porous media model with traditional porous media model

The traditional porous media models that are generally used for traditional packed beds includes the Attou, Lappalainen, Iliuta and Zhang models, which are shown in the Appendix. To compare the new model with traditional models, the Burns and Yang experimental sets of data are employed with E_1 = 180 and E_2 = 1.8 (E_1 and E_2 are the Ergun constants shown in the Appendix) for the Attou, Lappalainen and Iliuta models and 100 μm as the droplet size (Yan et al., 2014; Zhao et al., 2016) for the Zhang model.

In the experimental work of Burns, the liquid flow rate is 17.5 cm^3/s, the gas flow rate is 2.0 cm^3/s and the rotation angular speed is 600 rpm. The simulation results are shown in Fig. 10(a). Although the predicted results and the corresponding tendency obtained from these traditional models are similar to the experimental correlation, the simulated values for the liquid holdup are much lower than the experimental data. The error in the liquid holdup at the exit of the packed bed is 72.9%, 56.6%, 51.6% and 84.7%, respectively, for the Attou, Lappalainen, Iliuta and Zhang models, respectively. However, the error for the new model is within 13%.

For the experiment of Yang, the experimental condition with the liquid flow rate 22.9 cm^3/s and rotation speed 1500 rpm is used for assessing the different models. It can be seen from Fig. 10(b) that the liquid holdup predicted by these models are much lower than the experimental value, with errors up to in excess of 80%, but for the new model, the error is within 10%.

Therefore, on comparing the simulation and experimental results, these gas-liquid porous media models do not fit the real physical situation for the liquid flow in the RPB. The reason may be that the predicted liquid flow resistance in these models is too low. Comparing the Attou, Lappalainen, Iliuta and Zhang models, the new model is the best porous media model for predicting the liquid holdup distribution in rotating wire screen packed beds and different packing materials have different θ values.

4. Conclusions

In this paper, a new model based on the Kołodziej wire screen one-phase porous media model is proposed for the Eulerian simulation of the gas-liquid two-phase flow in RPBs. For this new model, the surface of the packing is divided into the wet surface and the dry surface, thus the drag forces between the liquid and solids and the gas and solids are obtained based on the wire size as the hydraulic diameter. As the gas flows through the wet surface area, the effect of the enlargement of the wire size by the covered liquid is considered for the drag force between gas and liquid.

Through validation using two experimental cases, it is demonstrated that the new model is very successful in describing the liquid flows in RPBs when employing the Eulerian method. Values of θ (the angle of the flow direction to the bed axis) = 56.2° and 80.0° were obtained by validation with the experimental data of Burns

and Yang, respectively. In order to examine the effect of the angle of the flow direction to the bed axis (θ) and the new model further, different rotation speeds and liquid flow rates have been simulated.

Finally, through comparing the new model with the traditional porous media models, such as the Attou, Lappalainen, Iliuta and Zhang models for traditional packed beds, this work has clearly illustrated that the new model is very effective for predicting the liquid flow in RPBs. Further, it is the most appropriate and accurate model for wire screen packing among the different porous media models that have been investigated.

Acknowledgements

The authors would like to acknowledge the financial support provided by the Engineering and Physical Science Research Council (EPSRC) under grant EP/M001458/2. In addition, P. Xie would like to acknowledge the China Scholarship Council and the University of Sheffield for funding his research studies.

Appendix

(i) Attou model (Attou et al., 1999; Gunjal et al., 2005) (sphere packing)

Interaction drag force between the gas and liquid:

$$F_{GL}=\left(\frac{E_1\mu_G(1-\varepsilon_G)^2}{\varepsilon_G^2 d_p^2}\left(\frac{\varepsilon_S}{1-\varepsilon_G}\right)^{\frac{2}{3}}+\frac{E_2\rho_G|v_G-v_L|(1-\varepsilon_G)}{(1-\varepsilon_S)\varepsilon_G d_p}\left(\frac{\varepsilon_S}{1-\varepsilon_G}\right)^{\frac{1}{3}}\right)\times\frac{\varepsilon_G}{(1-\varepsilon_S)}(v_G-v_L) \tag{A.1}$$

Interaction drag force between the gas and solids:

$$F_{GS}=\left(\frac{E_1\mu_G(1-\varepsilon_G)^2}{\varepsilon_G^2 d_p^2}\left(\frac{\varepsilon_S}{1-\varepsilon_G}\right)^{\frac{2}{3}}+\frac{E_2\rho_G|v_G|(1-\varepsilon_G)}{(1-\varepsilon_S)\varepsilon_G d_p}\left(\frac{\varepsilon_S}{1-\varepsilon_G}\right)^{\frac{1}{3}}\right)\times\frac{\varepsilon_G}{(1-\varepsilon_S)}v_G \tag{A.2}$$

Interaction drag force between the liquid and solids:

$$F_{LS}=\left(\frac{E_1\mu_L\varepsilon_S^2}{\varepsilon_L^2 d_p^2}+\frac{E_2\rho_L|v_L|\varepsilon_S}{(1-\varepsilon_S)\varepsilon_L d_p}\right)\frac{\varepsilon_L}{(1-\varepsilon_S)}v_L \tag{A.3}$$

(ii) Lappalainen model (Lappalainen et al., 2008, 2009) (sphere packing)

$$F_{GL}=\left(\frac{E_{\mu,G}(1-\varepsilon_G)^2\mu_G}{\varepsilon_G^2 d_p^2}+\frac{E_{\rho,G}(1-\varepsilon_G)\rho_G|v_G-\alpha_{gs}v_L|}{\alpha_{gs}(1-\varepsilon_S)\varepsilon_G d_p}\right)\frac{\varepsilon_G}{\alpha_{gs}(1-\varepsilon_S)}\times(v_G-\alpha_{gs}v_L) \tag{A.4}$$

$$F_{GS}=\left(\frac{E_{\mu,G}(1-\varepsilon_G)^2\mu_G}{\varepsilon_G^2 d_p^2}+\frac{E_{\rho,G}(1-\varepsilon_G)\rho_G|v_G|}{\alpha_{gs}(1-\varepsilon_S)\varepsilon_G d_p}\right)\frac{\varepsilon_G}{\alpha_{gs}(1-\varepsilon_S)}v_G \tag{A.5}$$

$$F_{LS}=\left(\frac{E_{\mu,G}\varepsilon_S^2\mu_L}{\varepsilon_L^2 d_p^2}+\frac{E_{\rho,L}\varepsilon_S\rho_L|v_L|}{(1-\varepsilon_S)\varepsilon_L d_p}\right)\frac{\varepsilon_L}{(1-\varepsilon_S)}v_L \tag{A.6}$$

$$T_0=\sqrt{\frac{72}{E_1}},\quad T_G=\frac{T_0+1}{2}+\alpha_{gs}\left(\frac{T_0+1}{2}-1\right),\quad T_L=T_0\cdot 3.592^{\alpha^{1.140}} \tag{A.7}$$

$$E_{\mu,i}=72T_i^2,\quad E_{\rho,i}=6f_\tau T_i^3,\quad f_\tau=E_2/(6T_0^3),\quad \alpha_{gs}=\frac{\varepsilon_G}{1-\varepsilon_S} \tag{A.8}$$

(iii) Iliuta model (Iliuta et al., 2004) (structured slit packing)

$$F_{GL}=f_e\left(\frac{E_1}{36}\frac{a_S^2\mu_G}{(1-\varepsilon_S)^2\left(1-\frac{\varepsilon_L}{f_e}\right)^2}+\frac{E_2}{6}\frac{a_S\rho_G\varepsilon_G}{(1-\varepsilon_S)\left(1-\frac{\varepsilon_L}{f_e}\right)^2}\times\left|v_G-v_L+\frac{\varepsilon_L\left(1-\frac{1}{f_e}\right)}{\varepsilon_G}v_L\right|\right)\left(v_G-v_L+\frac{\varepsilon_L\left(1-\frac{1}{f_e}\right)}{\varepsilon_G}v_L\right)\varepsilon_G \tag{A.9}$$

$$F_{LS}=f_e\left(\frac{E_1}{36}\frac{a_S^2\mu_L f_e}{\varepsilon_L^3}+\frac{E_2}{6}\frac{a_S}{\varepsilon_L^3}\rho_L|v_L|\right)v_L\varepsilon_L \tag{A.10}$$

$$F_{GS}=(1-f_e)\left(\frac{E_1}{36}\frac{a_S^2\mu_G}{(1-\varepsilon_S)^3}+\frac{E_2}{6}\frac{a_S}{(1-\varepsilon_S)^3}\rho_G|v_G|\right)v_G(1-\varepsilon_S) \tag{A.11}$$

(iv) Zhang and Bokil's model (Zhang and Bokil, 1997) (tube bundle packing)

$$F_{GL}=C_f(v_G-v_L) \tag{A.12}$$

$$C_f=\frac{1}{2}\rho_G f_d A_d\frac{1}{(1-\varepsilon_S)}|v_G-v_L| \tag{A.13}$$

$$A_d=\frac{1.5R_lV}{D_d} \tag{A.14}$$

$$F_{GS}=\xi_G\rho_G v_G v_{p,G} \tag{A.15}$$

$$\xi_G=2\left(\frac{f_G}{P_t}\right)\left(\frac{P_t\beta}{P_t-D_o}\right)^2\left(\frac{1-\beta}{1-\beta_t}\right)\left(\frac{1}{1-\varepsilon_S}\right)^2 \tag{A.16}$$

$$F_{LS}=\xi_L\rho_L v_L v_{p,L} \tag{A.17}$$

$$\xi_L=2\left(\frac{f_L}{P_t}\right)\left(\frac{P_t\beta}{P_t-D_o}\right)^2\left(\frac{1-\beta}{1-\beta_t}\right)\left(\frac{1}{1-\varepsilon_S}\right)^2 \tag{A.18}$$

$$f_i=0.619Re^{-0.198}\quad Re<8000 \tag{A.19}$$

$$f_i=1.156Re^{-0.2647}\quad Re\geqslant 8000 \text{ and } Re<200000 \tag{A.20}$$

References

Al-Fulaij, H., Cipollina, A., Micale, G., 2014. Eulerian-Eulerian modelling and computational fluid dynamics simulation of wire mesh demisters in MSF plants. Eng. Comput. 31, 1242–1260.

Attou, A., Boyer, C., Ferschneider, G., 1999. Modelling of the hydrodynamics of the concurrent gas-liquid trickle flow through a trickle-bed reactor. Chem. Eng. Sci. 54, 785–802.

Bašić, A., Duduković, M.P., 1995. Liquid holdup in rotating packed beds: examination of the film flow assumption. AIChE J. 41, 301–316.

Burns, J.R., Jamil, J.N., Ramshaw, C., 2000. Process intensification: operating characteristics of rotating packed beds-determination of liquid hold-up for a high voidage structured packing. Chem. Eng. Sci. 55, 2401–2415.

Bussière, W., Rochette, D., Clain, S., André, P., Renard, J.B., 2017. Pressure drop measurements for woven metal mesh screens used in electrical safety switchgears. Int. J. Heat Fluid Flow 65, 60–72.

Chandra, A., Goswami, P.S., Rao, D.P., 2005. Characteristics of flow in a rotating packed bed (HIGEE) with split packing. Ind. Eng. Chem. Res. 44, 4051–4060.

Chang, C.C., Chiu, C.Y., Chang, C.Y., Chang, C.F., Chen, Y.H., Ji, D.R., Yu, Y.H., Chiang, P. C., 2009. Combined photolysis and catalytic ozonation of dimethyl phthalate in a high-gravity rotating packed bed. J. Hazard. Mater. 161, 287–293.

Chen, J.F., Shao, L., Guo, F., Wang, X.M., 2003. Synthesis of nanofibers of aluminium hydroxide in novel rotating packed bed reactor. Chem. Eng. Sci. 58, 569–575.

Chen, Y.H., Huang, Y.H., Lin, R.H., Shang, N.C., 2010. A continuous-flow biodiesel production process using a rotating packed bed. Bioresour. Technol. 101, 668–673.

Chen, Y.S., Liu, H.S., Lin, C.C., Liu, W.T., 2004. Micromixing in a rotating packed bed. J. Chem. Eng. Jpn. 37, 1122–1128.
Chen, Y.S., Lin, F.Y., Lin, C.C., Tai, C.Y.D., Liu, H.S., 2006. Packing characteristics for mass transfer in a rotating packed bed. Ind. Eng. Chem. Res. 45, 6846–6853.
Chen, Y.S., Lin, C.C., Liu, H.S., 2011. Mass transfer in a rotating packed bed with various radii of the bed. Ind. Eng. Chem. Res. 50, 1778–1785.
Dijkhuizen, W., Roghair, I., Van Sint Annaland, M., Kuipers, J.A.M., 2010. DNS of gas bubbles behavior using an improved 3D front tracking model-Drag force on isolated bubbles and comparison with experiments. Chem. Eng. Sci. 65, 1415–1426.
Fourati, M., Roig, V., Raynal, L., 2013. Liquid dispersion in packed columns: Experiments and numerical modeling. Chem. Eng. Sci. 100, 266–278.
Gunjal, P.R., Kashid, M.V., Ranade, V.V., Chaudhari, R.V., 2005. Hydrodynamics of trickle-bed reactors: experiments and CFD modeling. Ind. Eng. Chem. Res. 44, 6278–6294.
Guo, F., Zheng, C., Guo, K., Feng, Y., Gardner, N.C., 1997. Hydrodynamics and mass transfer in cross-flow rotating packed bed. Chem. Eng. Sci. 52, 3853–3859.
Hassan-Beck, H.M., 1997. Process intensification: mass transfer and pressure drop for counter current rotating packed beds. PhD dissertation. University of Newcastle-upon-Tyne, UK.
Heidari, A., Hashemabadi, S.H., 2014. CFD simulation of isothermal diesel oil hydrodesulphurization and hydrodearomatization in trickle bed reactor. J. Taiwan Inst. Chem. Eng. 45, 1389–1402.
Iliuta, I., Petre, C.F., Larachi, F., 2004. Hydrodynamic continuum model for two-phase flow structured-packing-containing columns. Chem. Eng. Sci. 59, 879–888.
Jassim, M.S., Rochelle, G., Eimer, D., Ramshaw, C., 2007. Carbon dioxide absorption and desorption in aqueous monoethanolamine solutions in a rotating packed bed. Ind. Eng. Chem. Res. 46, 2823–2833.
Jiao, W.Z., Liu, Y.Z., Qi, G.S., 2010. Gas pressure drop and mass transfer characteristics in a cross-flow rotating packed bed with porous plate packing. Ind. Eng. Chem. Res. 49, 3732–3740.
Jindal, A., Buwa, V.V., 2017. Effect of bed characteristics on local liquid spreading in a trickle bed. AIChE J. 63, 347–357.
Joel, A.S., Wang, M., Ramshaw, C., Oko, E., 2014. Process analysis of intensified absorber for post-combustion CO_2 capture through modelling and simulation. Int. J. Greenhouse Gas Control 21, 91–100.
Kang, J.L., Sun, K., Wong, D.S.H., Jang, S.S., Tan, C.S., 2014. Modelling studies on absorption of CO_2 by monoethanolamine in rotating packed bed. Int. J. Greenhouse Gas Control 25, 141–150.
Kołodziej, A., Łojewska, J., 2009. Experimental and modelling study on flow resistance of wire gauzes. Chem. Eng. Process. 48, 816–822.
Kołodziej, A., Jaroszyński, M., Janus, B., Kleszcz, T., Łojewska, J., Łojewski, T., 2009. An experimental study of the pressure drop in fluid flows through wire gauzes. Chem. Eng. Comm. 196, 932–949.
Lappalainen, K., Alopaeus, V., Manninen, M., Aittamaa, J., 2008. Improved hydrodynamic model for wetting efficiency, pressure drop, and liquid holdup in trickle-bed reactors. Ind. Eng. Chem. Res. 47, 8436–8444.
Lappalainen, K., Manninen, M., Alopaeus, V., 2009. CFD modeling of radial spreading of flow in trickle-bed reactors due to mechanical and capillary dispersion. Chem. Eng. Sci. 64, 207–218.
Lashkarbolooki, M., 2017. A general model for pressure drop prediction across a rotating packed bed. Sep. Sci. Technol. 52, 1843–1851.
Li, X., Zhang, Y., Wang, X., Ge, W., 2013. GPU-based numerical simulation of multi-phase flow in porous media using multiple-relaxation-time lattice Boltzmann method. Chem. Eng. Sci. 102, 209–219.
Lin, C.C., Chen, Y.S., Liu, H.S., 2000. Prediction of liquid holdup in countercurrent-flow rotating packed bed. Chem. Eng. Res. Des. 78, 397–403.
Lin, C.C., Ho, T.J., Liu, W.T., 2002. Distillation in a rotating packed bed. J. Chem. Eng. Jpn. 35, 1298–1304.
Lin, C.C., Wei, T.Y., Hsu, S.K., Liu, W.T., 2006. Performance of a pilot-scale cross-flow rotating packed bed in removing VOCs from waste gas streams. Sep. Purif. Technol. 52, 274–279.
Lin, C.C., Chiang, Y.J., 2012. Feasibility of using a rotating packed bed in preparing coupled ZnO/SnO_2 photocatalysts. J. Ind. Eng. Chem. 18, 1233–1236.
Liu, Y., Luo, Y., Chu, G.W., Luo, J.Z., Arowo, M., Chen, J.F., 2017. 3D numerical simulation of a rotating packed bed with structured stainless steel wire mesh packing. Chem. Eng. Sci. 170, 365–377.
Lopes, R.J.G., Quinta-Ferreira, R.M., 2008. Three-dimensional numerical simulation of pressure drop and liquid holdup for high-pressure trickle-bed reactor. Chem. Eng. J. 145, 112–120.
Lopes, R.J.G., Quinta-Ferreira, R.M., 2009. Turbulence modelling of multiphase flow in high-pressure trickle-bed reactors. Chem. Eng. Sci. 64, 1806–1819.
Luo, Y., Chu, G.W., Zou, H.K., Zhao, Z.Q., Dudukovic, M.P., Chen, J.F., 2012. Gas-liquid effective interfacial area in a rotating packed bed. Ind. Eng. Chem. Res. 51, 16320–16325.
Onda, K., Takeuchi, H., Okumoto, Y., 1968. Mass transfer coefficients between gas and liquid phases in packed columns. J. Chem. Eng. Jpn. 1, 56–62.
Ouyang, Y., Zou, H., Gao, X., Chu, G., Xiang, Y., Chen, J., 2018. Computational fluid dynamics modelling of viscous liquid flow characteristics and end effect in rotating packed bed. Chem. Eng. Process. 123, 185–194.
Panda, M., Bhowal, A., Datta, S., 2011. Removal of hexavalent chromium by biosorption process in rotating packed bed. Environ. Sci. Technol. 45, 8460–8466.
Pham, D.A., Lim, Y., Jee, H., Ahn, E., Jung, Y., 2015. Porous media Eulerian computational fluid dynamics (CFD) model of amine absorber with structured-packing for CO_2 removal. Chem. Eng. Sci. 132, 259–270.
Qian, Z., Xu, L.B., Li, Z.H., Li, H., Guo, K., 2010. Selective absorption of H_2S from a gas mixture with CO_2 by aqueous N-methyldiethanolamine in a rotating packed bed. Ind. Eng. Chem. Res. 49, 6196–6203.
Ramshaw, C., Mallinson, R.H., 1981. Mass transfer process, U.S. Patent 4,283, 255.
Ramshaw, C., 1983. HIGEE distillation-an example of process intensification. Chem. Eng. 389, 13–14.
Saez, A.E., Carbonell, R.G., 1985. Hydrodynamic parameters for gas-liquid concurrent flow in packed beds. AIChE J. 31, 52–62.
Sankaranarayanan, K., Shan, X., Kevrekidis, I.G., Sundaresan, S., 1999. Bubble flow simulations with the lattice Boltzmann method. Chem. Eng. Sci. 54, 4817–4823.
Shi, X., Xiang, Y., Wen, L.X., Chen, J.F., 2013. CFD analysis of liquid phase flow in a rotating packed bed reactor. Chem. Eng. J. 228, 1040–1049.
Shu, S., Yang, N., 2013. Direct numerical simulation of bubble dynamics using phase-field model and lattice Boltzmann method. Ind. Eng. Chem. Res. 52, 11391–11403.
Solomenko, Z., Haroun, Y., Fourati, M., Larachi, F., Boyer, C., Augier, F., 2015. Liquid spreading in trickle-bed reactors: experiments and numerical simulations using Eulerian-Eulerian two fluid approach. Chem. Eng. Sci. 126, 698–710.
Sun, B.C., Wang, X.M., Chen, J.M., Chu, G.W., Chen, J.F., Shao, L., 2011. Synthesis of nano-$CaCO_3$ by simultaneous absorption of CO_2 and NH_3 into $CaCl_2$ solution in a rotating packed bed. Chem. Eng. J. 168, 731–736.
Xie, P., Lu, X., Yang, X., Ingham, D., Ma, L., Pourkashanian, M., 2017. Characteristics of liquid flow in a rotating packed bed for CO_2 capture: A CFD analysis. Chem. Eng. Sci. 172, 216–229.
Yan, Z.Y., Lin, C., Ruan, Q., 2014. Dynamics of droplets and mass transfer in a rotating packed bed. AIChE J. 60, 2705–2723.
Yang, H.J., Chu, G.W., Zhang, J.W., Shen, Z.G., Chen, J.F., 2005. Micromixing efficiency in a rotating packed bed: experiments and simulation. Ind. Eng. Chem. Res. 44, 7730–7737.
Yang, W., Wang, Y., Chen, J., Fei, W., 2010. Computational fluid dynamic simulation of fluid flow in a rotating packed bed. Chem. Eng. J. 156, 582–587.
Yang, Y., Xiang, Y., Chu, G., Zou, H., Luo, Y., Arowo, M., Chen, J.F., 2015. A noninvasive X-ray technique for determination of liquid holdup in a rotating packed bed. Chem. Eng. Sci. 138, 244–255.
Yang, Y., Xiang, Y., Chu, G., Zou, H., Sun, B., Arowo, M., Chen, J., 2016. CFD modelling of gas-liquid mass transfer process in a rotating packed bed. Chem. Eng. J. 294, 111–121.
Zhang, C., Bokil, A., 1997. A quasi-three-dimensional approach to simulate the two-phase fluid flow and heat transfer in condensers. Int. J. Heat Mass Transf. 40, 3537–3546.
Zhao, B., Tao, W., Zhong, M., Su, Y., Cui, G., 2016. Process, performance and modelling of CO_2 capture by chemical absorption using high gravity: a review. Renew. Sust. Energ. Rev. 65, 44–56.